GDCh

Research Articles

Angewandte
Chemie
International Edition
www.angewandte.org

VIP **Imaging Agents** *Very Important Paper*

Activity-based Photoacoustic Probes Reveal Elevated Intestinal MGL and FAAH Activity in a Murine Model of Obesity

Melissa Y. Lucero+, Sarah H. Gardner+, Anuj K. Yadav, Austin Borri, Zhenxiang Zhao, and Jefferson Chan*

Abstract: Obesity is a chronic health condition characterized by the accumulation of excessive body fat which can lead to and exacerbate cardiovascular disease, type-II diabetes, high blood pressure, and cancer through systemic inflammation. Unfortunately, visualizing key mediators of the inflammatory response, such as monoacylglycerol lipase (MGL) and fatty acid amide hydrolase (FAAH), in a selective manner is a profound challenge owing to an overlapping substrate scope that involves arachidonic acid (AA). Specifically, these enzymes work in concert to generate AA, which in the context of obesity, has been implicated to control appetite and energy metabolism. In this study, we developed the first selective activity-based sensing probes to detect MGL (PA-HD-MGL) and FAAH (PA-HD-FAAH) activity via photoacoustic imaging. Activation of PA-HD-MGL and PA-HD-FAAH by their target enzymes resulted in 1.74-fold and 1.59-fold signal enhancements, respectively. Due to their exceptional selectivity profiles and deep-tissue photoacoustic imaging capabilities, these probes were employed to measure MGL and FAAH activity in a murine model of obesity. Contrary to conflicting reports suggesting levels of MGL can be attenuated or elevated, our results support the latter. Indeed, we discovered a marked increase of both targets in the gastrointestinal tract. These key findings set the stage to uncover the role of the endocannabinoid pathway in obesity-mediated inflammation.

Introduction

By the year 2025, the World Health Organization has projected that over one billion people worldwide will be classified as obese, which is a condition characterized by the accumulation of excessive body fat.[1] An undesirable hallmark of obesity is the development of a chronic inflammatory state that can exacerbate various human diseases.[2] For instance, inflammation of the gastrointestinal (GI) tract can increase the risk of non-alcoholic fatty liver disease,[3] gastroesophageal reflux,[4] gallstones,[5] and colorectal cancer.[6] Inflammation that is linked to obesity is a complex process that results from the interaction between various pathways including nitric oxide (NO) signalling and the endocannabinoid system (ECS).[7] To further complicate efforts to decipher the molecular underpinnings of this interplay, individual components of the ECS (e.g., MGL and FAAH) have been implicated in contradictory roles (*vide infra*).[8] Unfortunately, methods such as immunohistochemical staining, that are traditionally employed to determine the expression levels of a given ECS enzyme,[9] do not report on enzyme activity which can be dramatically altered based on the availability of substrates, cofactors, as well as changes in the local tissue environment (e.g., pH fluxes).[10]

Recently, the principles of activity-based sensing (ABS) have been employed to develop an expansive suite of imaging probes to study various human pathologies including inflammation.[10,11] Unlike traditional probe design strategies that rely on stoichiometric binding events, the reactivity of an ABS probe can be fine-tuned to match the availability of a target, while simultaneously minimizing cross-reactivity with competing analytes. For instance, our group has developed probes to detect NO, a low abundance and highly reactive nitrogen species, in murine models of inflammation[12] and cancer.[11t,13] Likewise, we have also prepared an isoform-selective, fluorogenic ABS probe to monitor the activity of cyclooxygenase-2 (COX-2),[11j] an enzyme responsible for the synthesis of prostaglandin proinflammatory mediators in live cells.[14] It is noteworthy that the readout of an ABS probe can be varied depending on the intended application (cellular versus *in vivo* imaging).[11c] To study inflammation, we have identified photoacoustic (PA) imaging as one of the preferential modalities because the incident light needed for probe excitation must be diffused (for even illumination) and thus,

[*] M. Y. Lucero,+ A. K. Yadav, Z. Zhao, J. Chan
Department of Chemistry, University of Illinois at Urbana-Champaign
Urbana, IL 61801 (USA)
E-mail: jeffchan@illinois.edu

S. H. Gardner,+ A. Borri, J. Chan
Department of Biochemistry, University of Illinois at Urbana-Champaign
Urbana, IL 61801 (USA)

M. Y. Lucero,+ S. H. Gardner,+ A. K. Yadav, A. Borri, Z. Zhao, J. Chan
Beckman Institute for Advanced Science and Technology
Urbana, IL 61801 (USA)

[+] These authors contributed equally to this work.

can readily penetrate into deep tissue. Moreover, the soundwaves generated via thermoelastic relaxation can propagate through the body with minimal perturbation.[15] Together, these properties enable the acquisition of high-resolution images (micron) at depths up to 10 centimeters, an important property necessary to image deep-seated organ systems such as the GI tract.[16]

Despite major advances in this research area,[17] the development of selective acoustogenic substrates for mono-acylglycerol lipase (MGL) and fatty acid amide hydrolase (FAAH), two key enzymes in the ECS, have remained elusive. The lack of such probes is likely due to their overlapping substrate scope. Specifically, MGL is a serine hydrolase that catalyzes the breakdown of 2-arachidonoyl-glycerol to yield arachidonic acid (AA) and glycerol via ester bond hydrolysis. Similarly, FAAH affords AA, as well as ethanolamine, through amide bond cleavage. In this study, we report the design and synthesis of PA-HD-MGL and PA-HD-FAAH, the first ABS probes for detecting MGL and FAAH activity *in vivo* via PA imaging, respectively. Because AA is a precursor to various inflammatory mediators, MGL and FAAH have been implicated to be involved in the immune response. Additionally, AA has also been linked to energy metabolism and appetite,[8b,18] which has prompted us to employ these probes to explore how the activity of MGL and FAAH are impacted in the inflamed GI tract of obese animals.

Results and Discussion

Design and Synthesis of PA-HD-MGL and PA-HD-FAAH

The first criterion we considered when designing PA-HD-MGL and PA-HD-FAAH was to obtain excellent substrate specificity for their respective enzyme targets. Limiting cross-reactivity is essential for *in vivo* detection of MGL and FAAH because both enzymes are present in the GI tract. We hypothesized this could be achieved by appending AA to a PA reporter via an ester bond (MGL) or an amide linkage (FAAH). The second major criterion is the probes must be minimally perturbing to the system under investigation. The selection of a strong PA emitter was therefore prioritized since doing so would allow us to dose at notably lower concentrations. To this end, we proposed an initial design where AA was appended to PA-HD via the linkages discussed above. PA-HD is a newly developed congener of the classic hemicyanine dye (HD) platform[19] but differs in that it has been optimized for PA imaging (4.8-fold higher sensitivity at the same dye concentration).[20] However, the resulting first-generation probes we prepared self-assembled into unreactive micelle-like particles due to the positively charge dye and hydrophobic tail components (Figure S1). We hypothesized that by replacing the *N*-ethyl group (cLogP=16.3) with a *N*-propyl sulfonate moiety (cLogP= 9.4), reactivity would be restored because the inclusion of negatively charged arms should disfavor aggregation.

Briefly, the synthesis of both probes began from cyanine **1**, which was prepared from the indolium sulfonate precur-sor in 60 % yield. PA-HDs **2** and **3** were obtained from the corresponding retro-Knoevenagel reactions using 4-chloro-3-methoxybenzenethiol and 3-aminothiophenol, followed by acylation with arachidonoyl chloride to obtain **PA-HD-MGL** and **PA-HD-FAAH** in 80 % and 78 % yield, respectively (Figure 1). Of note, the *ortho*-chloro substituent featured in PA-HD-MGL was strategically installed to attenuate spontaneous hydrolysis of the ester. Previous work in similar dye systems have shown this modification led to enhance stability which was due to donation of the halogen lone pair electrons to the π* orbital of the adjacent carbonyl.[21]

Photophysical Characterization and in vitro Evaluation

Following synthesis, we sought to determine the photo-physical properties of PA-HD-MGL, PA-HD-FAAH, and their corresponding turned over products (**2** and **3**) to ensure each dye exhibited the desired properties for *in vivo* PA imaging. We calculated the PA brightness factor (PABF) by multiplying the extinction coefficient at the λ_{abs} by the term (one minus the fluorescent quantum yield (Φ_F)).[22] We previously found that PABF values $> 10^4$ were necessary to reduce the amount of dye administered to animals while still maintaining a high PA output. In the case of **2** and **3**, the large experimental PABFs ($\approx 10^5$ range) can be attributed to strategic selection of the PA-HD platform which is highly efficient at harvesting incident light. Additionally, we found the λ_{PA} (wavelength of maximum PA signal output) for **2** and **3** to be 740 nm and 730 nm, respectively (Figure 2a). Excitation of PA-HD-MGL and PA-HD-FAAH at these wavelengths result in the negligible production of sound-waves, and this corresponds to theoretical signal enhance-ments of 7.29-fold and 4.15-fold, respectively. Of note, the PA spectral traces shown in Figure 2b and 2c were obtained using densely formulated phantoms comprised of milk and agarose at high concentrations as a proxy for deep-tissue imaging.[23]

Prior to evaluating the responsiveness of PA-HD-MGL and PA-HD-FAAH toward their respective target enzymes, it was necessary to assess the hydrolytic stability of each probe under relevant *in vivo* conditions. Specifically, the pH of the gastrointestinal tract begins at 6.0 (duodenum) and gradually increases to 7.4 (terminal ileum). Upon exiting the small intestines, a second pH gradient is associated with the large intestines that range from 5.7 (caecum) to 6.7 (rectum).[24] Our analyses indicate there is minimal change in the signal intensity in this pH range and furthermore, extended incubation up to one hour (a typical *in vivo* imaging experiment is only 30 minutes) shows 0.30-fold decrease (Figure S2). We attribute the exceptional stability of this particular ester moiety to the inclusion of the *ortho*-chloro group. Likewise, the stability of PA-HD-FAAH was extraordinary even under basic conditions (Figure S3). Having determined the requisite baseline readings, we treated each probe with purified human MGL and FAAH (Figure S4 and S5). To our delight, MGL only activated PA-HD-MGL and FAAH selectively catalyzed the turnover of
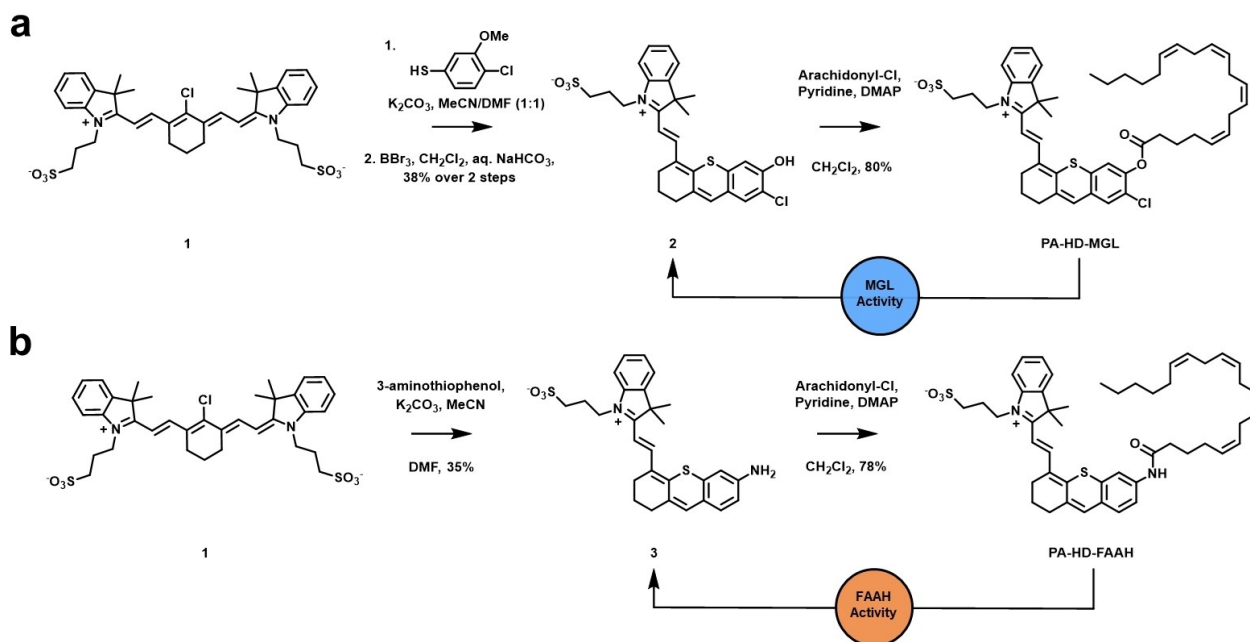
Figure 1. a) Synthesis of PA-HD-MGL and schematic illustrating MGL-catalysed activation to compound 2. b) Synthesis of PA-HD-FAAH and schematic illustrating FAAH-catalysed activation to compound 3.

PA-HD-FAAH. We confirmed the expected products were being generated via mass spectrometric analysis of probe samples treated with the appropriate enzyme (Figure S25 and S26). We attribute the absence of cross-reactivity between PA-HD-MGL and FAAH to enhanced stability to our *ortho*-chloro ester trigger. Indeed, FAAH has been shown to hydrolyze a variety of amide and ester substrates with nearly identical rates..[25] Beyond MGL and FAAH, we also subjected our probes to other enzymes including members of the ECS that recognizes AA as a substrate (cyclooxygenase-1, cyclooxygenase-2, and arachidonate 5-lipoxygenase),[26] various cytochrome p450s (via rat liver microsomes), ester bond cleaving enzymes (esterase and lipase), as well as catalase (Figure 2d and 2e). Under no circumstances did we observe notable off-target reactivity greater than 10 %. Lastly, we evaluated whether PA-HD-MGL and PA-HD-FAAH would turnover in the presence of biologically relevant analytes (Figure S6). No hydrolysis of the ester or amide bonds were observed in the presence of metal ions exhibiting Lewis acidic properties (i.e., iron and copper). We also found that PA-HD-MGL and PA-HD-FAAH were stable to nucleophiles such as thiols. Because the dye scaffold is susceptible to decomposition by reactive oxygen and nitrogen species, we also examined potential reactivity but found no change in the absorbance at biologically relevant concentrations of hydroxyl radical, superoxide, peroxynitrite, and nitric oxide.

Detection of MGL and FAAH Activity in Cell Cultures

Prior to utilizing PA-HD-MGL and PA-HD-FAAH *in vivo*, it is critical to demonstrate probe activation occurs selectively by the target enzyme in cell culture. A careful survey of the literature revealed that LNCaP cells (a human prostate adenocarcinoma cell line) constitutively express both MGL and FAAH at appreciable levels.[27] Moreover, we found the application of PA-HD-MGL, PA-HD-FAAH, and their corresponding turned over products at experimentally relevant concentrations and incubation periods did not significantly reduce LNCaP viability (Figure S7–10). Thus, we hypothesized treatment of this cell line with appropriate small-molecule inhibitors would allow us to determine the molecular target responsible for activating each probe. Specifically, JZL184,[28] a highly selective irreversible inhibitor of MGL, and PF-3845,[29] a potent FAAH covalent inhibitor that modifies the active site serine residue, were chosen for our studies. We began by pre-treating LNCaP cells with either a vehicle control or a solution of JZL184, prior to staining with PA-HD-MGL (Figure 3a and 3b). Our results demonstrate that blocking MGL activity using JZL184 led to a statistically significant decrease in fluorescence of 0.72 ± 0.08-fold (mean $\pm$ SEM) (Figure 3g). Importantly, we found that applying the FAAH inhibitor instead of JZL184 did not impact PA-HD-MGL activation, which provides further support that the signal enhancement is due to MGL activity (Figure 3c and S11). A similar set of experiments were performed to assess the responsiveness of PA-HD-FAAH in LNCaP cells. As before, cell cultures were treated with either a vehicle, PF-3845, or the MGL inhibitor. Consistent with our *in vitro* testing, attenuation of
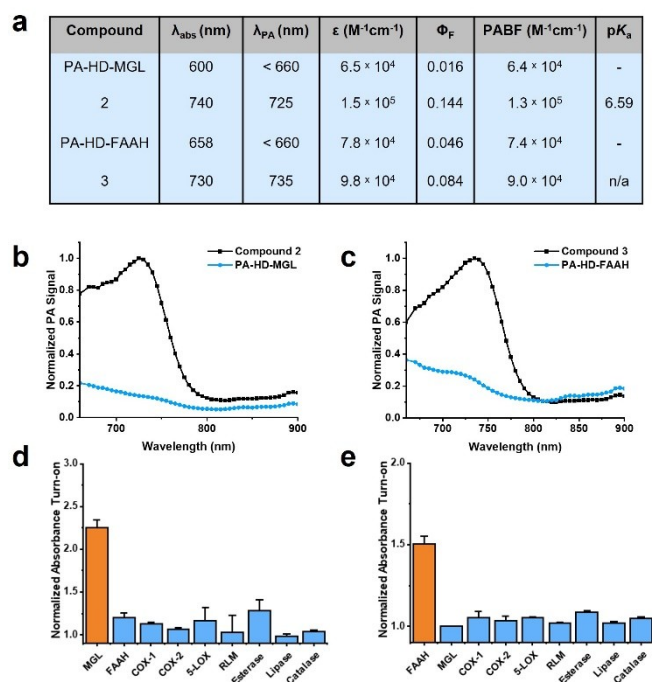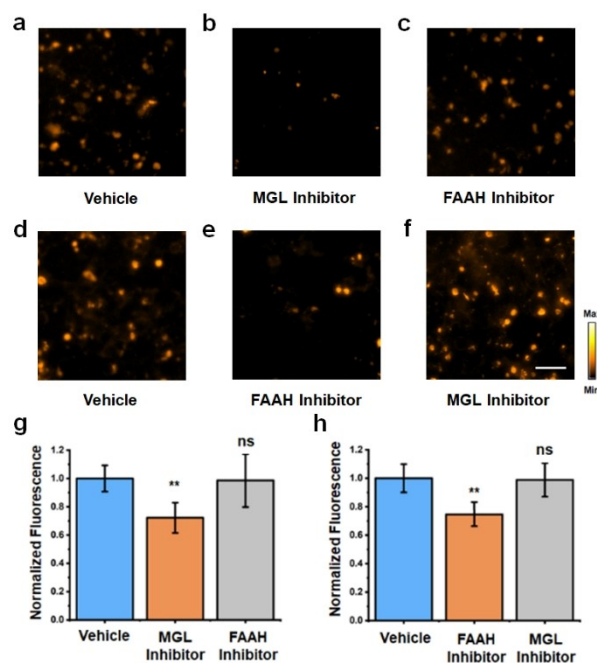
Figure 2. a) Summary of photophysical properties for PA-HD-MGL, compound 2, PA-HD-FAAH, and compound 3. Absorbance and PA maxima determined in 7:3 PBS:MeCN pH 7.4. Molar absorptivity coefficients and fluorescence quantum yields determined in DMSO. pKa were determined in 0.1% SDS in PBS (pH ranged from 2.7 to 11.8). b) PA spectra of compound 2 and PA-HD-MGL (10 µM, 7:3 PBS: MeCN, pH 7.4). c) PA spectra of compound 3 and PA-HD-FAAH (10 µM, 7:3 PBS:MeCN, pH 7.4). d) Fold absorbance turn-on of PA-HD-MGL in the presence of MGL, FAAH, COX-1, COX-2, 5-LOX, RLM, esterase, lipase or catalase after 15 minutes at optimal pH for respective enzymes in Tris buffer. e) Normalized absorbance turn-on of PA-HD-FAAH in the presence of FAAH, MGL, COX-1, COX-2, 5-LOX, RLM, esterase, lipase or catalase after 15 minutes at optimal pH for respective enzymes in Tris buffer.

Figure 3. Fluorescent images of PA-HD-MGL turn-on in LNCaP cells treated with a) vehicle control, b) MGL inhibitor, or c) FAAH inhibitor using PA-HD-MGL. Fluorescent images of PA-HD-FAAH turn-on in LNCaP cells treated with d) vehicle control, e) FAAH inhibitor, or f) MGL inhibitor using PA-HD-FAAH. MGL inhibitor = JZL184 (40 µM). FAAH inhibitor = PF-3845 (40 µM). Scale bar represents 50 µm. g) Quantification of data in a), b), and c). h) Quantification of data in d), e), and f). Statistical analysis was performed using a two-tailed Student's t-test ($\alpha = 0.05$), **$P < 0.01$, *$P < 0.05$, ns = not significant.

probe activation was only observed when FAAH activity was blocked via inhibition (0.75 ± 0.06-fold difference (mean $\pm$ SEM)) (Figure 3d–f, 3h and S12). Lastly, in addition to live cell imaging, we performed a series of cell lysate experiments. LNCaP cells were lysed via sonication, and serial dilutions of these lysates were generated and treated with either PA-HD-MGL or PA-HD-FAAH for a total of 30 and 90 minutes, respectively (Figure S13 and S14). In both instances, probe activation was shown to be dose-dependent where the most pronounced turnover was associated with samples containing the highest cell count.

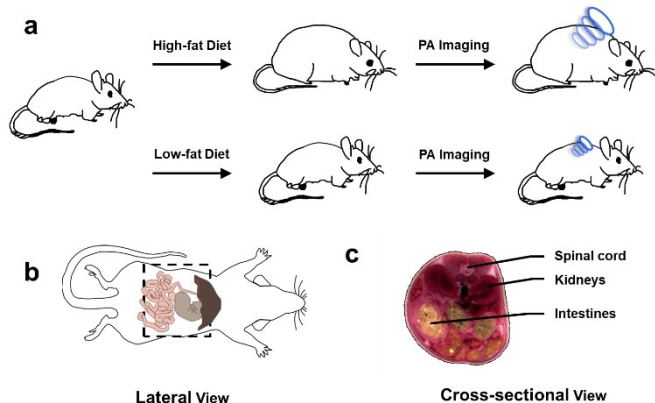### *In vivo* PA Imaging of MGL and FAAH Activity in a Murine Model of Obesity

Next, we established a murine model of obesity by feeding BALB/c mice (female, ≈ six weeks old) research-grade chow where fat accounts for 60% of the caloric profile for 12 weeks. Of note, female mice were selected to be consistent with a previous study conducted by our group to

assess diet-induced inflammation of the mammary fat pad.[11t] A second cohort of animals were fed a control diet where the calories from fat were standardized to only 10%. Although the chows are isocaloric, we found that by allowing the animals to feed freely, subjects on a high-fat diet became obese, gaining an average of 15.5% body weight over this period (Figure 4a). Since obesity is known to trigger an inflammatory response in the GI tract, we hypothesized the application of PA-HD-MGL and PA-HD-FAAH would allow us to discern how and to what extent this process involves the ECS. To facilitate *in vivo* PA imaging of the GI tract using our probes, which is a deep-seated region of the body, we turned to the use of an advanced MSOT (multispectral optoacoustic (photoacoustic) tomography) system because it is possible to visualize the entire animal and present the data in lateral and cross-sectional views (Figure 4b and 4c). Moreover, the PA signals from each probe (and their products) can be isolated from endogenous PA-active pigments such as hemoglobin found in blood and from each other via spectral unmixing.

PA-HD-MGL was then administered systemically via intraperitoneal injection to both groups of mice and the corresponding PA images were acquired at the 30-minute time point. Analysis of the spectrally unmixed images in lateral and cross-sectional views indicated PA signals corresponding to the turned over product was being

Angew. Chem. Int. Ed. **2022**, *61*, e202211774 (4 of 7)

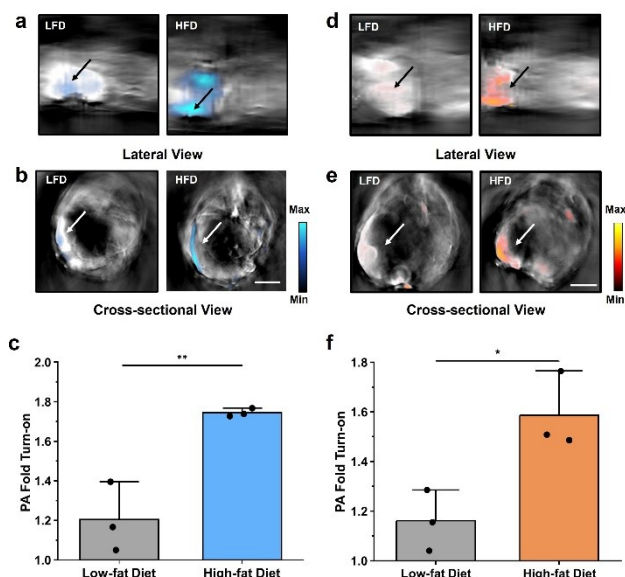© 2022 The Authors. Angewandte Chemie International Edition published by Wiley-VCH GmbH

Figure 4. a) Schematic representing workflow for the generation of murine models to study the effect of diet on MGL and FAAH activity using *in vivo* photoacoustic imaging. b) Lateral schematic of a mouse where the field of view is indicated by the dotted box. c) Cross-sectional schematic of a mouse to reference the positioning of the spinal cord, kidneys, and intestines.

Figure 5. Representative MSOT images showing the a) lateral and b) cross-sectional views of mice fed low-fat and high-fat diets treated with PA-HD-MGL (200 µM, 200 µL DMSO in saline). c) Average PA fold turn-on from MSOT imaging ($n=3$, independent animals). Representative MSOT images showing the d) lateral and e) cross-sectional views of mice fed low-fat and high-fat diets treated with PA-HD-FAAH (200 µM, 200 µL DMSO in saline). f) Average PA fold turn-on from MSOT imaging ($n=3$, independent animals). All images were acquired 0.5 h post-injection of the probe. All images shown are spectrally unmixed to show probe activation (in cyan for MGL and orange for FAAH) and arrow indicates intestines. Scale bar represents 5 mm. Statistical analysis was performed using a two-tailed *t*-test ($\alpha=0.05$, ** $P<0.01$).

generated. Moreover, the signals were isolated to the intestines. However, the strength of the signal output was 1.74-fold in the high-fat group compared to the low-fat animals, which was significantly lower (Figure 5a–c). This result indicates inflammation of the gastrointestinal tract in obese animals is linked to the upregulation of MGL activity.[8a,30] We corroborated our findings by excising intestines from sacrificed subjects for *ex vivo* PA imaging. Consistent with our *in vivo* data, the PA signal was greater in intestines from the high-fat diet group (Figure S15). On the contrary, the same PA pattern was not observed in other tissues (e.g., liver) that were analyzed. In these organ systems, there was no discernible difference in the PA signal between the two experimental groups (Figure S16). Having successfully demonstrated MGL activity is elevated in the obesity model, we turned our attention to uncover whether FAAH activity was altered in a similar manner. As before, both groups of animals were treated with PA-HD-FAAH and imaged using our MSOT system. Analysis of the data revealed comparable results to when PA-HD-MGL was employed. Specifically, we found the enhancement was greatest in the high-fat diet animals (1.59-fold signal enhancement) and PA signals originated from the gastro-intestinal tract (Figure 5d–f). The corresponding *ex vivo* validation studies confirmed our *in vivo* results (Figure S17 and S18).

Conclusion

ABS probes for enzymatic systems have emerged as powerful chemical tools for basic scientific and biomedical research owing to their ability to selectively report on the activity (rather than expression level) of a protein target. When equipped with an appropriate signal readout such as PA, it is possible to study an enzyme within an intact living organism (e.g., mouse). This is critically important for

enzymes involved in mediating an inflammatory response because their activity can be altered dramatically based on changes in the local tissue microenvironment. Prior to work presented in this study, such tools did not exist to monitor MGL and FAAH activity for deep tissue applications via PA imaging. A possible reason is concern over potential cross-reactivity because both targets feature a pocket that recognizes and binds to AA. While amide bonds are typically resistant to esterase activity (FAAH was not expected to react with PA-HD-MGL), the same is not true with regards to ester stability. Indeed, FAAH has been shown to mediate the hydrolysis of amide and ester substrates with nearly identical catalytic efficiencies.[25a] The most common strategy to stabilize an ester is to simply increase the steric bulk around the bond. For instance, pivaloyl esters are more stable than smaller methyl esters. However, this approach would require the chemical modification of AA, which will undoubtedly impact enzyme binding. Instead, we leveraged molecular orbital interactions to impart stability through the installation of a halide *ortho* to the phenoxide leaving group. It is remarkable that a single atom substitution (Cl for H) can eliminate nearly all cross-reactivity with FAAH, highlighting the incredible utility of ABS probe design strategies.

Beyond our efforts to achieve the requisite enzyme selectivity to distinguish between MGL and FAAH *in vivo*, we also explored strategies to optimize detection sensitivity. While PA imaging is characterized by the unique ability to detect ultrasound signals in deep tissue with high resolution, a PA probe must contend with an abundance of PA-active pigments such as hemoglobin found in blood that can increase the background. We addressed these concerns by employing PA-HD, which is a remodeled version of the canonical HDs featuring a notably stronger PA output. By doing so, we estimate we were able to reduce the amount of imaging probe administered by over 100 % relative to comparable systems using the parent HD.[31] Limiting the amount of PA-HD-MGL or PA-HD-FAAH introduced to an animal is important because AA is released in the process of probe activation which at higher levels may perturb the very biology we are trying to study.

In this regard, we observed strong ultrasound production localized to the GI tract of obese mice for both sets of imaging experiments. Spectral unmixing allowed us to unambiguously assign the signal to the corresponding turned over dye products. Because our probes are selective for their respective target enzymes, we were able to demonstrate for the first time that MGL and FAAH activity are elevated relative to control animals at a normal body weight. Without selective probes, attributing imaging agent activation to a particular target would be impossible. An increase in MGL and FAAH activity is intriguing in the context of obesity because they have been shown to play contradictory roles in mediating appetite and fat storage.[8] Specifically, leptin, a hormone that regulates hunger cues has been shown to increase FAAH activity in animal models and human subjects. Higher FAAH levels should in theory result in the suppression of food intake. On the contrary, overexpression of MGL in the small intestine has been reported to alter endocannabinoid levels and whole-body energy balance, resulting in obesity.[8a] The notion that the activity of both enzymes increases, highlights their complex role in the context of obesity and inflammation (e.g., inflammation overrides hormonal signaling cues to control hunger).

Acknowledgements

Conflict of Interest

The authors declare no conflict of interest.

Data Availability Statement

The data that support the findings of this study are available from the corresponding author upon reasonable request.

Keywords: Activity-Based Sensing · Endocannabinoid System · Inflammation · Obesity · Photoacoustic Imaging

[1] World Obesity Day: "All countries significantly off track to meet 2025 WHO targets on Obesity", https://www.worldobesity.org/news/world-obesity-day-all-countries-significantly-off-track-to-meet-2025-who-targets-on-obesity).

[2] a) S. Emerenziani, M. P. L. Guarino, L. M. Trillo Asensio, A. Altomare, M. Ribolsi, P. Balestrieri, M. Cicala, *Nutrients* **2019**, *12*, 111; b) S. P. Bapat, C. Whitty, C. T. Mowery, Y. Liang, A. Yoo, Z. Jiang, M. C. Peters, L.-j. Zhang, I. Vogel, C. Zhou, V. Q. Nguyen, Z. Li, C. Chang, W. S. Zhu, A. T. Hastie, H. He, X. Ren, W. Qiu, S. G. Gayer, C. Liu, E. J. Choi, M. Fassett, J. N. Cohen, J. L. Sturgill, L. E. Crotty Alexander, J. M. Suh, C. Liddle, A. R. Atkins, R. T. Yu, M. Downes, S. Liu, B. S. Nikolajczyk, I.-K. Lee, E. Guttman-Yassky, K. M. Ansel, P. G. Woodruff, J. V. Fahy, D. Sheppard, R. L. Gallo, C. J. Ye, R. M. Evans, Y. Zheng, A. Marson, *Nature* **2022**, *604*, 337–342.

[3] E. Fabbrini, S. Sullivan, S. Klein, *Hepatology* **2010**, *51*, 679–689.

[4] H. B. El-Serag, A. P. Thrift, in *The Esophagus* **2021**, pp. 624–632.

[5] L. Bonfrate, D. Q. H. Wang, G. Garruti, P. Portincasa, *Best Pract. Res. Clin. Gastroenterol.* **2014**, *28*, 623–635.

[6] a) L. J. Bou Malhab, W. M. Abdel-Rahman, *Curr. Mol. Pharmacol.* **2022**, *15*, 620–646; b) T. Deng, C. J. Lyon, S. Bergin, M. A. Caligiuri, W. A. Hsueh, *Annu. Rev. Pathol.* **2016**, *11*, 421–449.

[7] a) M. S. Ellulu, I. Patimah, H. Khaza'ai, A. Rahmat, Y. Abed, *Arch. Med. Sci.* **2017**, *13*, 851–863; b) T. V. Rohm, D. T. Meier, J. M. Olefsky, M. Y. Donath, *Immunity* **2022**, *55*, 31–55.

[8] a) S. H. Chon, J. D. Douglass, Y. X. Zhou, N. Malik, J. L. Dixon, A. Brinker, L. Quadro, J. Storch, *PLoS One* **2012**, *7*, e43962; b) G. Balsevich, M. Sticht, N. P. Bowles, A. Singh, T. T. Y. Lee, Z. Li, P. K. Chelikani, F. S. Lee, S. L. Borgland, C. J. Hillard, B. S. McEwen, M. N. Hill, *Proc. Natl. Acad. Sci. USA* **2018**, *115*, 7605–7610.

[9] a) M. P. Patricelli, J. E. Patterson, D. L. Boger, B. F. Cravatt, *Bioorg. Med. Chem. Lett.* **1998**, *8*, 613–618; b) E. Y. Dotsey, K. M. Jung, A. Basit, D. Wei, J. Daglian, F. Vacondio, A. Armirotti, M. Mor, D. Piomelli, *Chem. Biol.* **2015**, *22*, 619–628.

[10] S. H. Gardner, C. J. Reinhardt, J. Chan, *Angew. Chem. Int. Ed.* **2021**, *60*, 5000–5009; *Angew. Chem.* **2021**, *133*, 5052–5062.

[11] a) J. Chan, S. C. Dodani, C. J. Chang, *Nat. Chem.* **2012**, *4*, 973–984; b) K. J. Bruemmer, S. W. M. Crossley, C. J. Chang, *Angew. Chem. Int. Ed.* **2020**, *59*, 13734–13762; *Angew. Chem.* **2020**, *132*, 13838–13867; c) A. K. East, M. Y. Lucero, J. Chan, *Chem. Sci.* **2021**, *12*, 3393–3405; d) Z. Mao, J. Xiong, P. Wang,

J. An, F. Zhang, Z. Liu, J. Seung Kim, *Coord. Chem. Rev.* **2022**, *454*, 214356; e) I. Abd-Elrahman, H. Kosuge, T. Wises Sadan, Y. Ben-Nun, K. Meir, C. Rubinstein, M. Bogyo, M. V. McConnell, G. Blum, *PLoS One* **2016**, *11*, e0160522; f) C. Anorma, J. Hedhli, T. E. Bearrood, N. W. Pino, S. H. Gardner, H. Inaba, P. Zhang, Y. Li, D. Feng, S. E. Dibrell, K. A. Kilian, L. W. Dobrucki, T. M. Fan, J. Chan, *ACS Cent. Sci.* **2018**, *4*, 1045–1055; g) K. J. Bruemmer, O. Green, T. A. Su, D. Shabat, C. J. Chang, *Angew. Chem. Int. Ed.* **2018**, *57*, 7508–7512; *Angew. Chem.* **2018**, *130*, 7630–7634; h) C. Y.-S. Chung, J. M. Posimo, S. Lee, T. Tsang, J. M. Davis, D. C. Brady, C. J. Chang, *Proc. Natl. Acad. Sci. USA* **2019**, *116*, 18285–18294; i) K. Kailass, O. Sadovski, M. Capello, Y. a Kang, J. B. Fleming, S. M. Hanash, A. A. Beharry, *Chem. Sci.* **2019**, *10*, 8428–8437; j) A. K. Yadav, C. J. Reinhardt, A. S. Arango, H. C. Huff, L. Dong, M. G. Malkowski, A. Das, E. Tajkhorshid, J. Chan, *Angew. Chem. Int. Ed.* **2020**, *59*, 3307–3314; *Angew. Chem.* **2020**, *132*, 3333–3340; k) T. E. Bearrood, G. Aguirre-Figueroa, J. Chan, *Bioconjugate Chem.* **2020**, *31*, 224–228; l) J. Morstein, D. Höfler, K. Ueno, J. W. Jurss, R. R. Walvoord, K. J. Bruemmer, S. P. Rezgui, T. F. Brewer, M. Saitoe, B. W. Michel, C. J. Chang, *J. Am. Chem. Soc.* **2020**, *142*, 15917–15930; m) Y. He, J. Yu, X. Hu, S. Huang, L. Cai, L. Yang, H. Zhang, Y. Jiang, Y. Jia, H. Sun, *Chem. Commun.* **2020**, *56*, 13323–13326; n) Z. H. Yu, C. J. Reinhardt, T. H.-F. Wong, K. Y. Tong, J. Chan, H. Y. Au-Yeung, *Chem. Eur. J.* **2020**, *26*, 8794–8800; o) H. Iwashita, E. Castillo, M. S. Messina, R. A. Swanson, C. J. Chang, *Proc. Natl. Acad. Sci. USA* **2021**, *118*, e2018513118; p) R. A. Baglia, K. R. Mills, K. Mitra, J. N. Tutol, D. Ball, K. M. Page, J. Kallu, S. Gottipolu, S. D'Arcy, S. O. Nielsen, S. C. Dodani, *RSC Chem. Biol.* **2021**, *2*, 830–834; q) M. Y. Lucero, Y. Tang, C. J. Zhang, S. Su, J. A. Forzano, V. Garcia, X. Huang, D. Moreno, J. Chan, *Proc. Natl. Acad. Sci. USA* **2021**, *118*, e2106943118; r) P. Wang, L. Yu, J. Gong, J. Xiong, S. Zi, H. Xie, F. Zhang, Z. Mao, Z. Liu, J. S. Kim, *Angew. Chem. Int. Ed.* **2022**, *61*, e202206894; *Angew. Chem.* **2022**, *134*, e202206894; s) K. Hoshi, M. S. Messina, J. Ohata, C. Y.-S. Chung, C. J. Chang, *Nature Protocols* **2022**, *17*, 1691–1710; t) A. K. Yadav, M. C. Lee, M. Y. Lucero, S. Su, C. J. Reinhardt, J. Chan, *ACS Cent. Sci.* **2022**, *8*, 461–472.

[12] C. J. Reinhardt, E. Y. Zhou, M. D. Jorgensen, G. Partipilo, J. Chan, *J. Am. Chem. Soc.* **2018**, *140*, 1011–1018.

[13] a) C. J. Reinhardt, R. Xu, J. Chan, *Chem. Sci.* **2020**, *11*, 1587–1592; b) E. Y. Zhou, H. J. Knox, C. J. Reinhardt, G. Partipilo, M. J. Nilges, J. Chan, *J. Am. Chem. Soc.* **2018**, *140*, 11686–11697; c) M. Y. Lucero, A. K. East, C. J. Reinhardt, A. C. Sedgwick, S. Su, M. C. Lee, J. Chan, *J. Am. Chem. Soc.* **2021**, *143*, 7196–7202.

[14] L. S. Simon, *Am. J. Medicine* **1999**, *106*, 37S–42S.

[15] L. Li, L. V. Wang, *BME Frontiers* **2021**, *2021*, 9823268.

[16] L. V. Wang, J. Yao, *Nat. Methods* **2016**, *13*, 627–638.

[17] a) D. M. Mofford, S. T. Adams, G. S. K. K. Reddy, G. R. Reddy, S. C. Miller, *J. Am. Chem. Soc.* **2015**, *137*, 8684–8687; b) Y. Yuan, F. Wang, W. Tang, Z. Ding, L. Wang, L. Liang, Z. Zheng, H. Zhang, G. Liang, *ACS Nano* **2016**, *10*, 7147–7153; c) Z. Qiao, H. Zhang, Y. Zhang, K. Wang, *iScience* **2020**, *23*,

101294; d) R. Cheng, M. Fujinaga, J. Yang, J. Rong, A. Haider, D. Ogasawara, R. S. Van, T. Shao, Z. Chen, X. Zhang, E. R. Calderon Leon, Y. Zhang, W. Mori, K. Kumata, T. Yamasaki, L. Xie, S. Sun, L. Wang, C. Ran, Y. Shao, B. Cravatt, L. Josephson, M.-R. Zhang, S. H. Liang, *Acta Pharmacol. Sin.* **2022**; e) M. Miceli, S. Casati, P. Allevi, S. Berra, R. Ottria, P. Rota, B. R. Branchini, P. Ciuffreda, *Int. J. Mol. Sci.* **2021**, *22*, 6148.

[18] H. Tallima, R. El Ridi, *J. Adv. Res.* **2018**, *11*, 33–41.

[19] a) L. Yuan, W. Lin, S. Zhao, W. Gao, B. Chen, L. He, S. Zhu, *J. Am. Chem. Soc.* **2012**, *134*, 13510–13523; b) J. Huang, J. Li, Y. Lyu, Q. Miao, K. Pu, *Nat. Mater.* **2019**, *18*, 1133–1143; c) Z. Zeng, S. S. Liew, X. Wei, K. Pu, *Angew. Chem. Int. Ed.* **2021**, *60*, 26454–26475; *Angew. Chem.* **2021**, *133*, 26658–26679.

[20] S. H. Gardner, C. J. Brady, C. Keeton, A. K. Yadav, S. C. Mallojjala, M. Y. Lucero, S. Su, Z. Yu, J. S. Hirschi, L. M. Mirica, J. Chan, *Angew. Chem. Int. Ed.* **2021**, *60*, 18860–18866; *Angew. Chem.* **2021**, *133*, 19008–19014.

[21] a) W. Chyan, H. R. Kilgore, B. Gold, R. T. Raines, *J. Org. Chem.* **2017**, *82*, 4297–4304; b) N. W. Pino, J. Davis 3rd, Z. Yu, J. Chan, *J. Am. Chem. Soc.* **2017**, *139*, 18476–18479.

[22] E. Y. Zhou, H. J. Knox, C. Liu, W. Zhao, J. Chan, *J. Am. Chem. Soc.* **2019**, *141*, 17601–17609.

[23] H. Li, P. Zhang, L. P. Smaga, R. A. Hoffman, J. Chan, *J. Am. Chem. Soc.* **2015**, *137*, 15628–15631.

[24] J. Fallingborg, *Dan. Med. Bull.* **1999**, *46*, 183–196.

[25] a) M. P. Patricelli, B. F. Cravatt, *Biochemistry* **1999**, *38*, 14125–14130; b) D. L. Boger, R. A. Fecik, J. E. Patterson, H. Miyauchi, M. P. Patricelli, B. F. Cravatt, *Bioorg. Med. Chem. Lett.* **2000**, *10*, 2613–2616.

[26] V. S. Hanna, E. A. A. Hafez, *J. Adv. Res.* **2018**, *11*, 23–32.

[27] L. Ruiz-Llorente, S. Ortega-Gutiérrez, A. Viso, M. G. Sánchez, A. M. Sánchez, C. Fernández, J. A. Ramos, C. Hillard, M. A. Lasunción, M. L. López-Rodríguez, I. Díaz-Laviada, *Br. J. Pharmacol.* **2004**, *141*, 457–467.

[28] J. Z. Long, W. Li, L. Booker, J. J. Burston, S. G. Kinsey, J. E. Schlosburg, F. J. Pavón, A. M. Serrano, D. E. Selley, L. H. Parsons, A. H. Lichtman, B. F. Cravatt, *Nat. Chem. Biol.* **2009**, *5*, 37–44.

[29] K. Ahn, D. S. Johnson, M. Mileni, D. Beidler, J. Z. Long, M. K. McKinney, E. Weerapana, N. Sadagopan, M. Liimatta, S. E. Smith, S. Lazerwith, C. Stiff, S. Kamtekar, K. Bhattacharya, Y. Zhang, S. Swaney, K. Van Becelaere, R. C. Stevens, B. F. Cravatt, *Chem. Biol.* **2009**, *16*, 411–420.

[30] K. Yoshida, Y. Kita, S. M. Tokuoka, F. Hamano, M. Yamazaki, K. Sakimura, M. Kano, T. Shimizu, *FASEB J.* **2019**, *33*, 2484–2497.

[31] Q. Li, S. Li, S. He, W. Chen, P. Cheng, Y. Zhang, Q. Miao, K. Pu, *Angew. Chem. Int. Ed.* **2020**, *59*, 6941–6941; *Angew. Chem.* **2020**, *132*, 7005–7005.